International Journal of Microwave and Wireless Technologies

cambridge.org/mrf

Single layer miniaturized ultra-thin FSS with five closely spaced bands

Anupam Dey[1] and Rajarshi Sanyal[2]

[1]Calcutta Institute of Technology, NH6, Banitabla, Uluberia, Howrah, West Bengal 711316, India and [2]MCKV Institute of engineering, 243, G T Road North, Liluah, Howrah, West Bengal 711204, India

Research Paper

Cite this article: Dey A, Sanyal R (2019). Single layer miniaturized ultra-thin FSS with five closely spaced bands. *International Journal of Microwave and Wireless Technologies* **11**, 797–805. https://doi.org/10.1017/S1759078719000370

Received: 22 October 2018
Revised: 12 March 2019
Accepted: 13 March 2019
First published online: 3 May 2019

Key words:
Octagonal interconnected loops; ultrathin FSS; five bands; unit cell miniaturization

Author for correspondence:
Anupam Dey,
E-mail: anupam.dey107@gmail.com

Abstract

This Paper reveals a novel single layer five band frequency selective surface (FSS). Novelties of the proposed FSS lie in its five closely spaced stop bands at 2.4, 3.38, 4.82, 6.32, and 7.75 GHz as well as the reduced single layer structural thickness (0.0016 λ_0) and the miniaturized unit cell size (0.0656 λ_0) at lower resonant frequency as compared to the existing multiband FSS. The unit cell structure consists of six octagonal concentric interconnected loops. Adjacent loop interconnection technique reduces the cell size by more than 44%. Furthermore, arrow-shaped rings are also introduced on each corner of the outermost octagonal loop, and using this technique approximate 23% cell miniaturization can be achieved. In addition, the proposed FSS exhibits excellent angular stability.

Introduction

Frequency selective surfaces (FSS) over the last decade are drawing considerable research attention due to their wide range of applications as spatial filters that can be used for selective transmission of specific frequency band while rejecting the others [1] in the domain of microwave and millimeter wave. Designs of multiband FSS have been intensively investigated due to the great demand of multiple independent transmission bands in wireless communication systems. In case of low frequency, closely located, narrowband operations like Wi-Fi, WIMAX, and WLAN, miniaturization of element size and reduction of frequency ratio (FR) are becoming a major concern. Several approaches regarding dual, tri or quad band FSS design [2–12] have been reported so far in earlier literatures. Substantial amount of work has also been reported [4–16] in the accomplishment of multiband FSS design.

To achieve multiple pass bands or stop bands with sufficient reduction in cell dimension and to obtain adjacent band FR with better angular stability, cascaded FSS designs with two or more metallic array are extensively reported in early works [2–7]. Cascading of complementary meandered structure with complementary grid structure [2] and a combination of complementary structures with spatial lumped element [3] have been investigated for dual layered tri-band application. Similarly, four branch spiral triangle, when convolved with gridded tortuous cross-dipole, three closely spaced bands can be obtained [4]. A new triple-layered FSS is realized for tri-band GSM application [5]. Moreover, multilayered fractal structure design provides X band application of FSS [6]. Another triple layer cascading technique involves two gridded triple square loop array cascaded with double square loop [7] resulting in highly selective quad band responses. However, the thicknesses of the aforementioned structures are too large to make the FSS suitable for practical applications. Such types of design optimization also suffer from the undesired mutual effect between each layer.

The ultra-thin single metallic sheet without any dielectric substrate may also provide quad band response [8]. A unit cell of that FSS has four square slots within which multiple stubs are loaded to provide close amount of band spacing. In another approach, close dual or tri-band response can be achieved by using three concentric split rings slots [9–10]. Closely packed concentric circular slots with narrow metallic short can redistribute the surface current that in turn minimizes the coupling effect upon which effective reduction in large band separation can be achieved. Another single layer ultrathin structure provides close dual band response for X band application where FSS unit cell is composed from centered square patch with L shaped arms [11]. The above literatures [8–11] reveal the mechanism to obtain close spaced multiband using single layer FSS due to their higher resonance frequency. However, effective cell miniaturization has not been confirmed yet. The miniaturization of cell size is another major issue for multiband FSS due to its wide employability in electromagnetic shielding for indoor communication [12]. The miniaturized crooked cross convoluted geometry has been discussed for single layer FSS with dual closely space bands [13]. In another work [14], a dual closely located stop band FSS with better miniaturization has been reported where the FSS comprises two convoluted meandered metallic strips in each quadrant of the unit cell connected through

© Cambridge University Press and the European Microwave Association 2019

CAMBRIDGE UNIVERSITY PRESS

a cross dipole. Another miniaturized dual band FSS unit cell design has been evolved from conventional patch slot topology [15].

In this paper, a miniaturized single layer five band FSS is presented. The miniaturized FSS unit element size is 0.065 $\lambda_{o1} \times$ 0.065 λ_{o1} large and 0.21 $\lambda_{05} \times 0.21$ λ_{05} large where λ_{01} and λ_{05} stands for the wavelength for lower and higher operating band. The metallic layer of unit cell geometry consists of six concentric octagonal narrow strips where adjacent octagonal metallic loops are interconnected to each other. In addition to this, four arrow-shaped meandered strips has been connected to the outer most loop. Employing the interconnection technique between the adjacent loops, 44% cell size reduction can be accomplished. Furthermore, increasing the effective electrical length of the proposed cell by incorporating arrow-shaped meandered line, 23% cell reduction has also been achieved. Besides, the substrate thickness in the proposed structure has been noticeably reduced by 45% due to the extremely thin dielectric material employed here. In addition, an impressive reduction in frequency band ratio has been observed where the minimum value is as low as 1.22. The proposed FSS can be utilized as a special kind of Band Stop Filter, which can be applicable in Wi-Fi, WLAN, and X band downlink satellite service.

Development of unit cell structure and simulated results

The proposed five band structure has been illustrated in Fig. 1. This proposed unit cell structure is derived from basic octagonal concentric sequential loop design with symmetrical arm length. Figure 2 illustrates step by step development to finalize the ultimate proposed structure. Each individual octagonal metallic strip acts as a resonating arm and its effective length is approximately $\lambda/2$ corresponding to the resonance. Besides the inductive loading of concentric octagonal patterns, another influencing factor is the uniform narrow spacing between adjoined metallic loops which causes strong capacitive effect. By exploiting the coupling mechanism and introducing the sixth concentric loop, a significant resonance shift towards lower frequency band (especially for the fifth band) can be achieved. As a result of that indicative reduction of unit cell dimension multiple to λ_{05} occurs, where λ_{05} is the wavelength corresponding to the fifth resonant frequency. However, due to the sequential coupling effect, slight shifting of first four resonant frequencies towards higher frequency range can be observed. Interactive coupling also reduces the FR between adjacent bands. In the next development, four beveled arm of the exterior octagonal strip connected to four symmetrical arrow-shaped printed metallic patterns. Meandered arrow-shaped patterns accommodate larger resonance length in smaller area which further increases the inductive effect. Captative effect due to enclosed space by arrow-shaped metallic ring also increases total capacitance value. As a result of that, better shifting of first resonance towards the lower frequency band can be observed as illustrated in Fig. 3 and Table 1. On the other hand, minor or negligible shifting can be observed for the other four resonances towards the lower frequency range. Unit cell also reduces from 0.154 λ_{01} to 0.118 λ_{01} where λ_{01} is the wavelength corresponding to the lower resonant frequency. Adjacent band ratio f_2/f_1 is considerably high because of the large resonance shifting of the first band compared to the second one. In the final development, neighboring loops are interconnected with each other with the help of narrow metallic conductors having a similar width. The proposed gridded loop structure is basically a meandering pattern

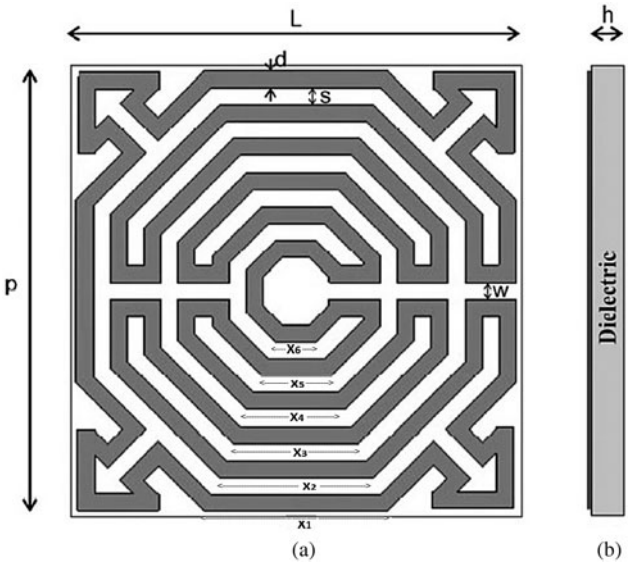

Fig. 1. Unit cell geometry of the proposed five band FSS.

with large effective electrical length which connects ad joint octagonal resonating elements and therefore produces a noticeable improvement for equivalent inductance and capacitance for all five resonant. Resonating arms for each stop band resonance are in sharing mode of the proposed meandered pattern. As shown in Fig. 4 it is observed that transmission zero shifts nearly from 18 to 22% corresponding to the first to fifth resonance with the variation of meandered gap d. Optimized dimension of the designed unit cell are given in mm: $L = 8.46$, $p = 8.2$, $W = 0.3$, $D = 0.3$, $S = 0.3$, $h = 0.2$ and the simulated results have been obtained by using CST microwave simulator. According to the analogy of transmission line theory, for a given length equivalent capacitance will be smaller for the wider gap between two parallel metallic strips. By varying gap width in between metallic strips, capacitive effect can be reduced which further increase the resonating frequencies.

Surface current analysis

To understand the significant resonance frequency shift towards the lower frequencies, surface current distribution analysis has been demonstrated and explained. Figure 5(a) illustrates the surface current distribution for concentric octagonal loop without interconnection and Fig. 5(b) shows the surface current distribution proposed interconnected concentric octagonal loop element at different resonance frequencies. The monopole like current distribution can be observed for all the five resonance frequencies, if the adjacent octagonal loops are not interconnected with each other. Without interconnection, physically five individual loops are mainly responsible for the respective five resonances. Although the mutual coupling effect of the adjacent loop can also be seen due to the closer gap of successive loops, major responsibility lies on the individual loop and the effective surface current path is approximately equivalent to the quarter wavelength of its corresponding resonant frequency. As an example, the current distribution at 4.32 GHz can be seen especially along the outermost loop and arrow-shaped rings; similarly, the surface current at 22.51 GHz is mainly concentrated around the fifth ring. The minor current concentration to the adjacent ring

https://doi.org/10.1017/S1759078719000370 Published online by Cambridge University Press

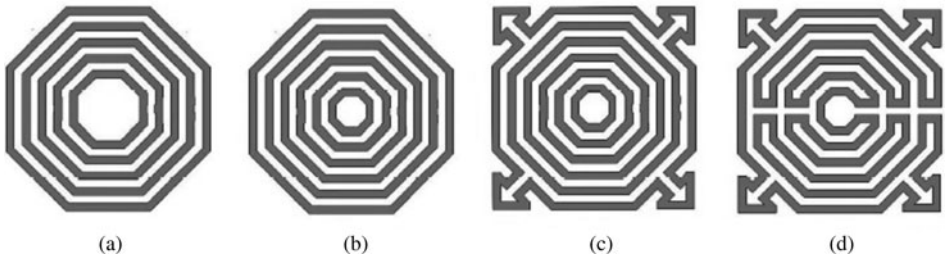

Fig. 2. Sequential development of unit cell. (a) Configuration-1 (five concentric octagonal loops). (b) Configuration-2 (six concentric octagonal loops). (c) Configuration-3 (six concentric octagonal loops with four arrow-shaped rings without interconnection). (d) Proposed configuration.

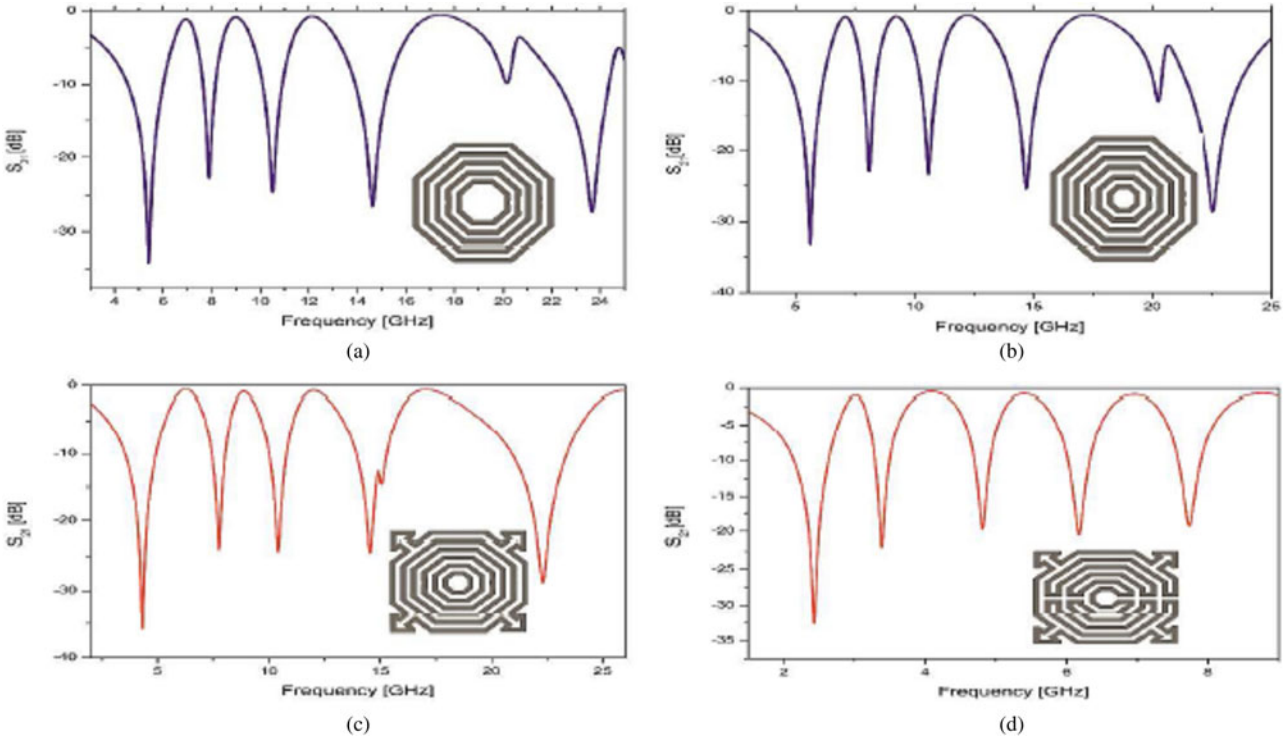

Fig. 3. Transmission response of different configuration. (a) Configuration-1. (b) Configuration-2. (c) Configuration-3. (d) Proposed configuration.

occurs due to the mutual effect of the adjacent ring. On the other hand, intentional interconnection between adjacent loops demonstrates dipole like surface current distribution. Impressive improvement of the traveling current path can be clearly observed for each resonant frequency in Fig. 5(b). An enlargement of effective current path which is approximated to half-wavelength at its corresponding frequency makes remarkable enhancement of equivalent inductance. Larger equivalent inductance leads to lowering of resonance frequencies. Thus, the smaller element size is achieved. Without interconnection between the adjacent concentric loops, there will be a strong interaction among the vertical surface currents at the narrow capacitive spacing between two adjacent metallic strips. Due to this strong mutual coupling, the adjacent frequency band shifts away. Consequently, the higher FR between the adjacent bands can be observed. However, in proposed cell geometry, asymmetrical current distribution reduces the coupling effect between the adjacent loops, causing the close band-spacing.

Furthermore, evaluating the surface current for each resonant frequency, an equivalent circuit model can be realized. The surface current at 2.4 GHz is mainly concentrated on the three outermost loops as shown in Fig. 5(b) through the interconnection. Excited surface current of the parallel lines are oppositely directed thereby forming a series connection. Interconnection produces length enhancement of effective meandered pattern which further increases the effective inductance. The closer gap between adjacent metallic loops produces a strong coupling effect which produces a large capacitive effect and consequently lowers the resonant frequency. Similarly, at 3.38, 4.82, 6.32, and 7.75 GHz impressive improvement of inductive length occurs due to the interconnection of successive inner loops

Equivalent circuit extraction and analysis

The proposed lumped equivalent model has been represented by a series LC circuit, with characteristics impedance z_0, across the transmission line for all the five resonant frequencies as shown in Fig. 6. As it is hard to realize an accurate model of the proposed complex FSS structure, an estimation of the lumped parameters like inductance (L) and capacitance (C) from the proposed structure becomes a challenging problem. However, adopting the hypothesis of approximate structural equalization between

https://doi.org/10.1017/S1759078719000370 Published online by Cambridge University Press

Table 1. Development of proposed configuration

Design	Operating frequencies (GHz)	Unit cell size correspond-ing to 1st resonance	Unit cell size correspond-ing to 5th resonance	Adjacent band ratio				Mini-mum Band Ratio
				f_2/f_1	f_3/f_2	f_4/f_3	f_5/f_4	
FSS-1	5.46, 7.73, 10.51, 14.62, 25.91	0.149 λ_{01}	0.713 λ_{05}	1.41	1.35	1.39	1.77	1.35
FSS-2	5.61, 8.09, 10.65, 14.68, 22.53	0.154 λ_{01}	0.616 λ_{05}	1.44	1.31	1.37	1.54	1.31
FSS-3	4.32,7.93,10.49,14.61, 22.51	0.118 λ_{01}	0.616 λ_{05}	1.83	1.32	1.39	1.54	1.32
Proposed FSS	2.40, 3.38, 4.82, 6.32, 7.75	0.0656 λ_{01}	0.215 λ_{05}	1.40	1.42	1.31	1.22	1.22

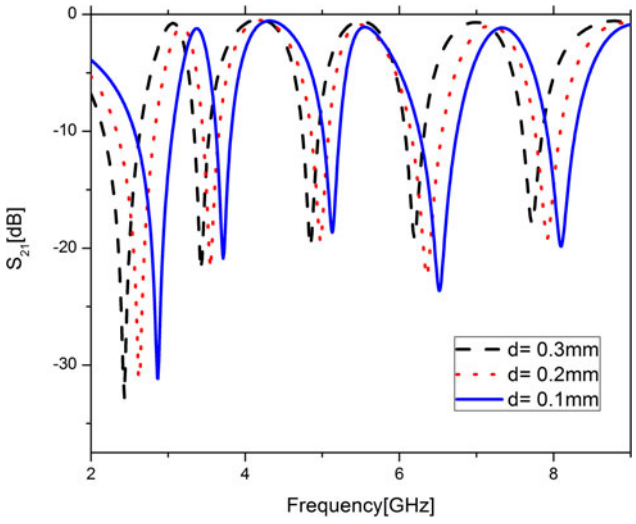

Fig. 4. Variation of transmission response with different "*d*".

symmetrical octagonal strip and circular ring conducting loop [17] and exploiting the surface current analysis from Fig. 5 for each resonance frequency, adequate synthesis and simplified formulation of circuit elements can be provided with fair level of accuracy.

In this paper, the equivalent circuit analysis has been organized in two sections. The first section comprises synthesis procedure of *L*-*C* equivalent circuit from the desired filtering response as depicted in Fig. 6. The subsequent section offers a relationship between the equivalent circuit parameters and the physical dimension of the proposed FSS.

Synthesis of the Effective *L*–*C* circuit model of the proposed microwave filter can be done by exploiting the contiguous surface current distribution. In early synthesis, it is assumed that the octagonal strips are independent without any metallic short and thereby the effective inductance (L_1–L_6) can be approximated to be proportional to the corresponding octagonal conductor length (X_1–X_6). Further, the successive loop interconnection providing the inductive nature of metal short produces a meandered strip line and the series connection between successive inductors. On the contrary, capacitance (C_1–C_6) of the circuit model which completely depends on the width of gap between the conducting strips and neighboring unit cell, forms parallel connection. To simplify the analysis, mutual coupling between the metallic strip and capacitive effect inside the arrow-shaped ring resonators as well as the capacitive gap between the meandered line have not been considered.

Since for each stopband resonance frequency, inductance enhances due to the enlargement of the metallic pattern, the meandered line has profound effects on capacitance as illustrated and as well explained in surface current distribution analysis. Therefore, the resonant frequencies of five stop bands can be roughly expressed as

$$f_{r1} = \frac{1}{2\pi\sqrt{(L_1 + L_2 + L_3)C_{eq1}}}, \tag{1}$$

$$f_{r2} = \frac{1}{2\pi\sqrt{(L_1/4 + L_2 + L_3 + L_4/4)C_{eq2}}}, \tag{2}$$

$$f_{r3} = \frac{1}{2\pi\sqrt{(L_3 + L_2/2 + L_4/2)Ceq_3}}, \tag{3}$$

$$f_{r4} = \frac{1}{2\pi\sqrt{(L_4 + L_3/2 + L_5/2)Ceq_4}}, \tag{4}$$

$$f_{r5} = \frac{1}{2\pi\sqrt{(L_4 + L_5 + L_6/2)Ceq_5}}, \tag{5}$$

where different sets of effective inductances (L_1–L_6)and capacitance (C_{eq1}–C_{eq5}) values have been shown in equation (1)–(5) corresponding to the resonant frequencies.

The equivalent capacitor is the sum of capacitive effect of the gap between successive octagonal rings. Using the surface current distribution analogy Equivalent capacitance C_{eq1}–C_{eq5} may be expressed as

$$C_{eq1} = C_1 + C_2 + C_3\,, \tag{6}$$

$$C_{eq2} = C_2 + C_3 + C_4, \tag{7}$$

$$C_{eq3} = C_3 + C_4, \tag{8}$$

https://doi.org/10.1017/S1759078719000370 Published online by Cambridge University Press

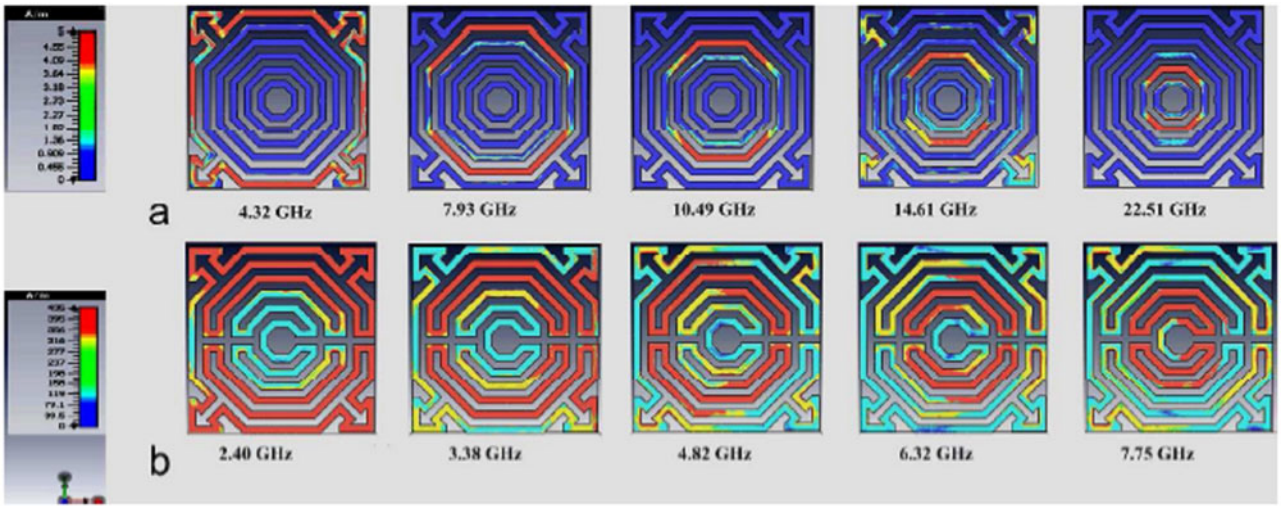

Fig. 5. (a)Surface current distribution for different frequencies without interconnection. (b) Surface crrent distribution for different frequencies with interconnection.

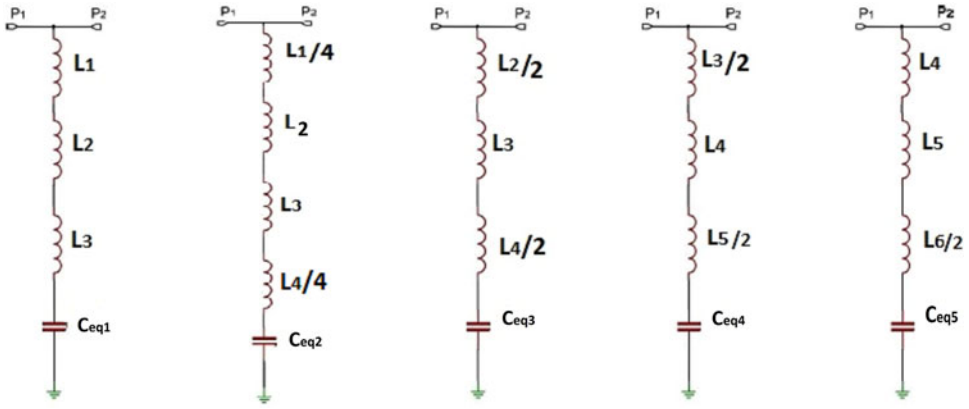

Fig. 6. Equivalent circuits of FSS. at (a) 2.4 GHz. (b) 3.38 GHz. (c) 4.82 GHz. (d) 6.32 GHz. (e) 7.75 GHz.

$$C_{eq4} = C_4 + C_5, \tag{9}$$

$$C_{eq5} = C_5 + C_6. \tag{10}$$

Multiple simulations have been performed in ADS to extract the values of L and C which can be derived as: $L_1 = 21.02$ nH, $L_2 = 12.6$ nH, $L_3 = 8.37$ nH, $L_4 = 7.6$ nH, $L_5 = 6.4$ nH, $L_6 = 3.2$ nH, $C_{eq1} = 104.5$ fF, $C_{eq2} = 79$ fF, $C_{eq3} = 59.1$ fF, $C_{eq4} = 44.1$ fF, and $C_{eq5} = 27.1$ fF. It can be found that weakening of the capacitive effect corresponds to the higher frequency because of the descending gap circumference among inner conductor loops.

Next section deals with the mapping between equivalent circuit model parameters and physical dimension of the proposed FSS structure where the selection of octagonal loop structure is the best compromise between the circular loop [17] and the straight-line square loop [18–20]. The development of the proposed design comprises the following steps. Initially, six concentric octagonal loops have been designed. In the next step, as four slant arms of outermost loops are interconnected with four triangular loops, an enlargement of outer periphery in limited space of unit cell occurs a significant phenomenon occurring in case of the circular equivalent polygon structure. Finally, adjacent octagonal rings are interconnected with each other. The parameters of the proposed interconnected loop structure are listed in Table 1. In order to map the equivalent circuit model parameters to the physical dimension of proposed unit cell structure, Marcuvitz modeling technique for periodic array of thin conducting strip has been used [21]. To estimate the equivalent inductance and capacitance of the concentric octagonal loop-shaped FSS structures, following basic equations [17] have been used:

$$\begin{aligned} L_1\omega_r &= 2 \times \frac{6X_1}{p} \times \frac{F(p,d,\lambda).F(p,d,\lambda)}{F(p,d,\lambda) + F(p,d,\lambda)} \\ &= \frac{12X_1}{p} \times \frac{F(p,d,\lambda)}{2} \end{aligned} \tag{11}$$

$$L_2\omega_r = \frac{4X_2}{p} F(p, 2d, \lambda), \tag{12}$$

https://doi.org/10.1017/S1759078719000370 Published online by Cambridge University Press

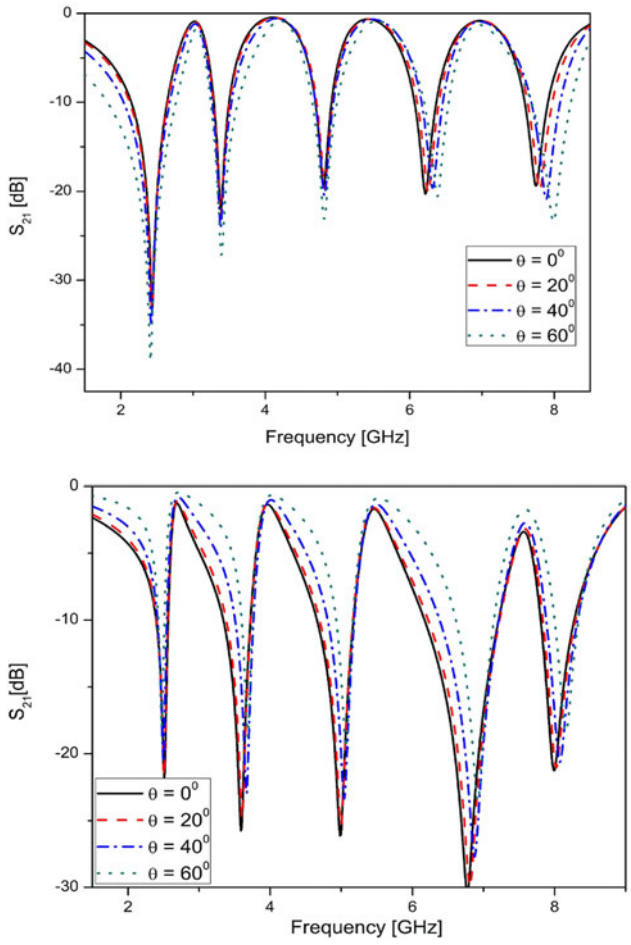

Fig. 7. Simulated transmission coefficient of proposed FSS structure under different incident angle. (a) TE polarization. (b) TM polarization.

$$L_i\omega_r = \frac{4X_i}{p}F(p, 2d, \lambda), , \tag{13}$$

$$C_1\omega_r = 0.75 \times 4\,\varepsilon_{eff}F(p, g_a, \lambda) \times \frac{3X_1}{p} = \frac{9X_1}{p}\,\varepsilon_{eff}F(p, g_a, \lambda), \tag{14}$$

$$C_2\omega_r = \frac{2X_2}{p}4\varepsilon_{eff}\frac{F(p, g_a, \lambda).F(p, g_a, \lambda)}{F(p, g_a, \lambda) + F(p, g_a, \lambda)}, \tag{15}$$

$$C_i\omega_r = \frac{2X_i}{p} \times 4\varepsilon_{eff} \times \frac{F(p, s, \lambda).F(p, s, \lambda)}{F(p, s, \lambda) + F(p, s, \lambda)} = 8\frac{X_i\varepsilon_{eff}}{p} \times \frac{F(p, s, \lambda)}{2}, \tag{16}$$

where ε_{eff}, F, D, p, d, s, and g_a correspond to the effective dielectric permittivity of the media, correction factor for the associated inductance and capacitance, size of the unit cell, gap between the outer loop parallel arm, width of the octagonal metallic strip, gap between successive loops, and effective gap of the unit cell, respectively. The quantity $g_a = D–p$ whereas X_1 and X_2 denote the arm length of most exterior and second most exterior arm length, respectively, X_i is the arm length of successive octagonal loops with $i = 3, 4, 5, 6$.

One arrow-shaped structure perimeter has been considered to be one arm length of X_1.

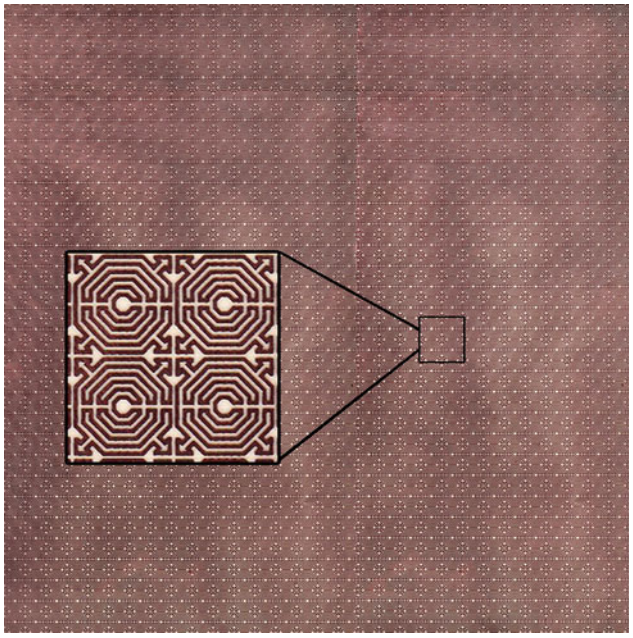

Fig. 8. Photograph of fabricated FSS prototype.

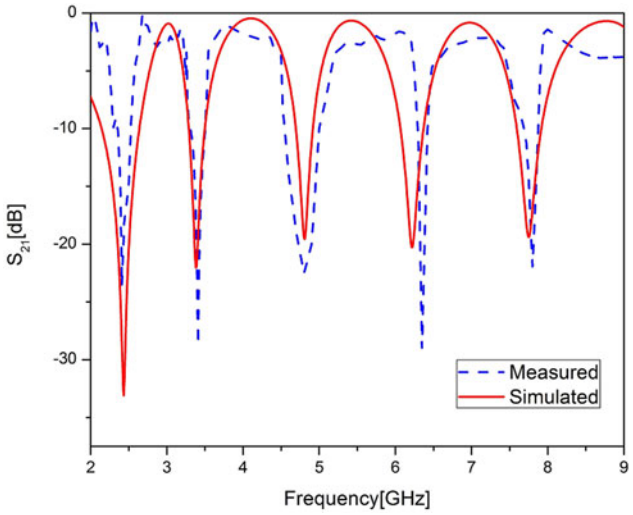

Fig. 9. Simulated and measured S-parameter under normal incidence.

Angular stability

Figure 7 illustrates transmission coefficient of the proposed FSS for TE and TM polarization under various oblique indent angles. It can be observed that under the large variation of incident angle ($0° \leq \theta \leq 60°$) at a step of 20°, stop bands for TE polarization

https://doi.org/10.1017/S1759078719000370 Published online by Cambridge University Press

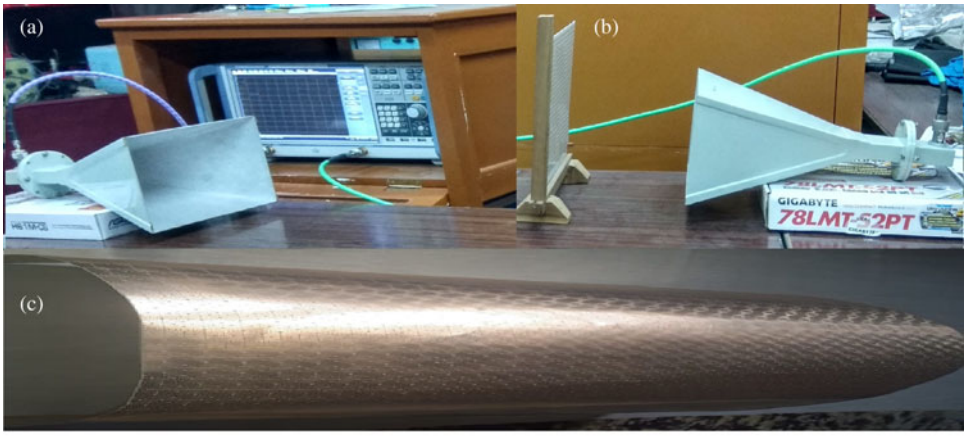

Fig. 10. (a) and (b) Experimental setup in free space (c) colded prototype.

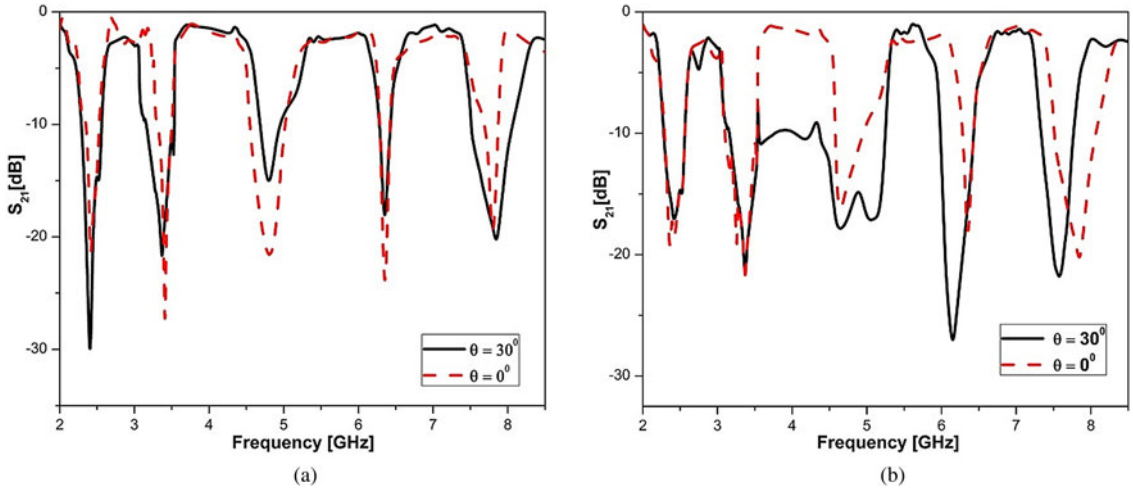

Fig. 11. Measured polarization (a) TE and (b) TM in different angles..

deviate slightly as 0.4, 0.26, 0.38, 2.27, and 2.45%, respectively. On the other hand, TM polarization deviations are 1.2, 1.9, 1.3, 2.1, and 2% corresponding to the five successive stop bands. However, still the proposed FSS provides acceptable resonance deviation <2.5% within the allowable limits. Bedsides bandwidth of TE waves slightly increases whereas bandwidth of TM wave decreases with respect to the increment of incident angle from 0° to 60°. These changes are mainly caused by variation of wave impedance as discussed in [22].

Experimental verification

To validate the simulated results of proposed structure, a prototype has been fabricated on FR-4 substrate having relative permittivity $\epsilon_r = 4.4$, loss tangent $tan\delta = 0.02$, and thickness h = 0.2 mm. prototype dimension is 320×320 mm^2, containing 38×38 elements as shown in Fig. 8. Transmission coefficient measurement of fabricated FSS has been carried out using two horn antennas connected to network analyzer (Rohde & Schwarz ZND20). a relatively good agreement between simulated and measured result has been observed in Fig. 9. Free space measurement setup is shown in Fig. 10. Two types of horn antennas pair has been used sequentially. Initially, large size Horn Antenna pair is used with frequency handling capacity of 2–3 GHz. Another Horn Antenna pair with operating frequency range 3–8 GHz used in next measurement. Due to the ultra-thin and flexible nature of the proposed prototype as observed in Fig. 10(c), prototype is attached carefully with the air foam sheet for measurement support. Moreover angular stability have been validated for the proposed structure. Transmission coefficient S_{21} of the different oblique incident angle at $\theta = 0°$ and $\theta = 30°$ have been carried out. Figure 11(a) shows TE polarization variation of the structure Fig. 11(b) shows TM polarization variation of the proposed structure. Both experimental responses show its parity with simulated results for both the angles.

Conclusion

A new miniaturized ultrathin FSS with five closely spaced stop bands is investigated numerically and experimentally. Adjacent loop interconnection technique is illustrated and demonstrated through the developed benchmark design. The proposed design has shown a convenient way to achieve five band FSS with multiple distinctive features such as compact ($0.0656\ \lambda_0 \times 0.0656\ \lambda_0$)

https://doi.org/10.1017/S1759078719000370 Published online by Cambridge University Press

Table 2. Comparison with existing multiband FSSs

FSS structure	No. of metallic layers	Resonant frequency(GHz)	Thickness of structure	Unit cell size	Adjacent band ratio(minimum)
This paper	Single	2.4, 3.38, 4.82, 6.32, 7.75	0.0016 λ_l	0.0656 λ_l	1.22
Ref. [7]	Three	7.7, 12.8, 18.8, 26.5	0.0514 λ_l	0.12 λ_l	1.4
Ref. [8]	single	8.2, 9.05, 9.9, 11.20	0.2328 λ_l	0.32 λ_l	1.09
Ref. [16]	Single	0.94, 1.84, 2.14	0.0031 λ_l	0.156 λ_l	1.16
Ref. [10]	Single	27.3, 31.7, 36.2	0.0184 λ_l	0.12 λ_l	1.14
Ref. [4]	Two	3.28, 4.2, 5.4	0.0054 λ_l	0.066 λ_l	1.19
Ref. [14]	single	2.35, 3.05	0.0062 λ_l	0.0658 λ_l	1.29
Ref. [11]	single	8.47, 10.45	0.0215 λ_l	0.248 λ_l	1.23

unit cell and ultra-thin thickness of 0.0016 λ_0 at lower resonant frequency. Adjacent band ratio of five bands is also settled in close range with minimum value of 1.22. The frequency characteristics have been extensively analyzed by equivalent circuit model and surface current analysis. Table 2 confirms the excellence of the proposed design with some other multiband FSS design irrespective to the number of resonant frequencies, unit cell size miniaturization, and dielectric thickness reduction. In addition to these significant achievements, the proposed structure provides stable transmission performance under oblique incidence of 60° for both TE and TM polarization. Finally, a prototype has been fabricated and tested which exhibit satisfactory agreement with the simulated result.

References

1. **Munk BA** (2005) *Frequency Selective Surfaces: Theory and Design*. New York: Wiley.
2. **Li H and Cao Q** (2015) Design and analysis of a controllable miniaturized tri-band frequency selective surface. *Progress in Electromagnetics Research Letters* **52**, 105–112.
3. **Wang DS, Chang YM, Che WQ, Chin KS and Chow YL** (2013) A low-profile frequency selective surface with controllable triband characteristics. *IEEE Antennas and Wireless Propagation Letters* **12**, 468–471.
4. **Liu N, Sheng XJ, Fan JJ and Guo D** (2017) A miniaturized tri-band frequency selective surface based on convoluted design. *IEEE Antennas and Wireless Propagation Letters* **62**, 17–22.
5. **Doken B and Kartal M** (2016) Triple band frequency selective surface design for global system for mobile communication systems. *IET Microwave Antennas Propagation* **10**, 1154–1158.
6. **Li Y, Li L, Zhang Y and Zhao C** (2015) Design and synthesis of multilayer frequency selective surface based on antenna-filter-antenna using Minkowski fractal structures. *IEEE Transactions on Antennas and Propagation* **63**, 133–141.
7. **Yan M, Wang J, Ma H, Qu S, Zhang J, Xu C, Zheng L and Zhang A** (2016) A quad-band frequency selective surface with highly selective characteristics. *IEEE Microwave and Wireless Components Letters* **26**, 562–564.
8. **Rahmati B and Hassani HR** (2015) Multi-band metallic frequency selective surface with wide range of band ratio. *IEEE Transactions on Antennas and Propagation* **63**, 3747–3753.
9. **Fabian-Gongora H, Martynyuk AE, Rodriguez-Cuevas J and Martinez-Lopez JI** (2015) Active dual-band frequency selective surfaces with close band spacing based on switchable ring slots. *IEEE Microwave and Wireless Components Letters* **25**, 606–608.
10. **Fabian-Gongora H, Martynyuk AE, Rodriguez-Cuevas J and Martinez-Lopez JI** (2016) Closely spaced tri-band frequency selective surfaces based on split ring slots. *Electronics letters* **52**, 727–729.
11. **Unaldı S, Cimen S, Cakır G and Ayten UE** (2017) A novel dual band ultra-thin FSS with closely settled frequency response. *IEEE Antennas and Wireless Propagation Letters* **16**, 1381–1384.
12. **Parker EA, Robertson J-B, Sanz-Izquierdo B and Batchelor JC** (2008) Minimal size FSS for long wavelength operation. IET *Electronics Letters* **44**, 394–395.
13. **Sivasamy R and Kanagasabai M** (2015) A novel dual-band angular independent FSS with closely spaced frequency response. *IEEE Microwave and Wireless Components Letters* **25**, 298–300.
14. **Ghosh S and Srivastava KV** (2017) An angularly stable dual-band FSS with closely spaced resonances using miniaturized unit cell. *IEEE Microwave and Wireless Components Letters* **27**, 218–220.
15. **Wdew AH, Riaz L, Naeem U and Shafique MF** (2017) A compact band-stop frequency selective surface for dual band Wi-Fi applications. *Microwave and Optical Technology Letters* **59**, 1920–1927.
16. **Kartal M, Golezani JJ and Doken B** (2017) A triple band frequency selective surface design for GSM systems by utilizing a novel synthetic resonator. *IEEE Transactions on Antennas and Propagation* **65**, 2724–2727.
17. **Ramezani Varkani A, Hossein Firouzeh Z and Zeidaabadi Nezhad A** (2018) Equivalent circuit model for array of circular loop FSS structures at oblique angles of incidence. *IET Microwaves, Antennas & Propagation* **12**, 749–755.
18. **Langley RJ and Parker EA** (1982) Equivalent circuit model for arrays of squareloops. *Electronics Letters* **18**, 294–296.
19. **Jha KR, Singh G and Jyoti R** (2012) A Simple Synthesis technique of Single layer square-loop Frequency selective Surface. *Progress in Electromagnetics Research B* **45**, 165–185.
20. **Yang J and Shen Z** (2007) A thin and broadband absorber using double-square loops. *IEEE Antennas and Wireless Propagation Letters* **6**, 388–391.
21. **Langley RJ and Drinkwater AJ** (1982) Improved empirical model for the Jerusalem cross. *Microwave, Antennas and Propagation, IEE Proceeding H* **129**, 1–6.
22. **Cimen S** (2013) Novel closely spaced planar dual-band frequency-selective surface. *IET Microwaves, Antennas & Propagation* **7**, 894–899.

Mr. Anupam Dey received his B.TECH and M.TECH degree in Electronics and Communication Engineering from WBUT in 2010 and 2014, respectively. Presently, he is working as an Assistant Professor in ECE department in Calcutta Institute of Technology, Howrah, West Bengal His main research interests are design and optimization of Microstrip Antenna and Frequency Selective Surfaces.

https://doi.org/10.1017/S1759078719000370 Published online by Cambridge University Press

Mr. Rajarshi Sanyal has obtained his AMIETE and M.Tech. Degree in Electronics and Communication. His area of Research Includes Microstrip Antenna and Microstrip filters. Presently, he is associated with MCKV Institute of Engineering as an Assistant Professor. He has presented and published various research papers in national and international journals.

https://doi.org/10.1017/S1759078719000370 Published online by Cambridge University Press